Electronic Supplementary Information for:

Enhancing organic photovoltaic performance with 3D-transport dual nonfullerene acceptors

Shuixing Dai,[a,*] Mengyang Li,[b] Jingming Xin,[c] Guanyu Lu,[d] Peiyao Xue,[e] Yong Zhao,[a] Yang Liu,[a] Mingliang Sun,[a] Liangmin Yu,[f] Zheng Tang,[b] Guanghao Lu,[d] Wei Ma [c] and Xiaowei Zhan[e,*]

[a] School of Materials Science and Engineering, Ocean University of China, Qingdao 266100, China. E-mail: daishuixing@ouc.edu.cn

[b] Center for Advanced Low-dimension Materials, State Key Laboratory for Modification of Chemical Fibers and Polymer Materials, College of Materials Science and Engineering, Donghua University, Shanghai 201620, China

[c] State Key Laboratory for Mechanical Behavior of Materials, Xi'an Jiaotong University, Xi'an 710049, China

[d] Frontier Institute of Science and Technology, Xi'an Jiaotong University, Xi'an 710054, China

[e] Key Laboratory of Polymer Chemistry and Physics of Ministry of Education, School of Materials Science and Engineering, Peking University, Beijing 100871, China. E-mail: xwzhan@pku.edu.cn

[f] Key Laboratory of Marine Chemistry Theory and Technology of Ministry of Education, Ocean University of China, Qingdao 266100, China

Materials. The chemical reagents and solvents used were obtained commercially and were used without further purification. PM6 and PDINO were purchased from Solarmer Materials Inc. and Suna Tech Inc., respectively. PEDOT:PSS (CLEVIOS P VP AI 4083) was purchased from J&K Scientific. FINIC was synthesized according to our published procedure.[1]

Measurements. UV-vis absorption spectra were recorded using a Shimadzu UV-1750 spectrophotometer in thin films (on a quartz substrate). Electrochemical measurements were measured under nitrogen in a deoxygenated solution of tetra-n-butylammonium hexafluorophosphate (0.1 M) in acetonitrile using a potential scan rate of 100 mV s^{-1} employing a computer-controlled CHI660E electrochemical workstation, a glassy-carbon working electrode coated with films, a platinum-wire auxiliary electrode, and an Ag/AgCl electrode as a reference electrode. The potentials were referenced to a ferrocenium/ferrocene ($FeCp_2^{+/0}$) couple using ferrocene as an external standard. The nanoscale morphology of the blends was observed employing an Agilent 5400 AFM in the tapping mode. Contact angle and surface tension measurements were performed on Dataphysics DCAT21.

Fabrication and characterization of OSCs. ITO glass (sheet resistance = 15 Ω) was precleaned successively in an ultrasonic bath using ultrapure water, acetone and isopropanol. Then the dried ITO were treated with UV/ozone for 3 min. PEDOT:PSS layer (*ca.* 30 nm) was spin coated at 4000 rpm onto the ITO substrates for 30 s, and baked at 150 °C for 15 min in air. For SHJ devices: PM6 (9 mg mL^{-1}) in chloroform was spin-coated at 1500 rpm on the PEDOT:PSS layer, then acceptor (10 mg mL^{-1}) in chloroform was spin-coated on the top of the PM6 layer at 3000 rpm to form a photoactive layer (*ca.* 100 nm). For BHJ devices:

PM6:acceptor (18.3 mg mL^{-1} in total; PM6:acceptor = 1:1.2, w/w) in chloroform was spin-coated at 3000 rpm on the PEDOT:PSS layer to form a photoactive layer (*ca.* 100 nm). The photoactive layers were annealed at 100 °C for 10 min in N_2 atmosphere. Then PDINO layer (*ca.* 10 nm) was spin-coated on the active layer. Finally, Al (*ca.* 80 nm) was evaporated onto the surface of the PDINO layer under vacuum (*ca.* 10^{-5} Pa). The active area of the device was *ca.* 4 mm^2. The *J*-*V* curve was measured using a computer-controlled B2912A Precision Source/Measure Unit (Agilent Technologies). An XES-70S1 (SAN-EI Electric Co., Ltd.) solar simulator (AAA grade, 70 × 70 mm^2 photobeam size) coupled with AM 1.5 G solar spectrum filters was used as the light source, and the optical power at the sample was 100 mW cm^{-2}. A 2 × 2 cm^2 monocrystalline silicon reference cell (SRC-1000-TC-QZ) was purchased from VLSI Standards Inc. The EQE spectrum was measured using a Solar Cell Spectral Response Measurement System QE-R3011 (Enlitech Co., Ltd.). The light intensity at each wavelength was calibrated using a standard single crystal Si photovoltaic cell.

Mobility measurements. Electron-only devices for Y6, FINIC, Y6:FINIC pristine films and PM6:acceptor blended films were fabricated with ITO/ZnO/pristine or blended films/Al structures. Hole-only devices for PM6:acceptor blended films were fabricated with ITO/PEDOT:PSS/blended films/Au structures. For electron-only devices, ZnO (*ca.* 30 nm) was prepared onto pre-cleaned glass using the method reported before,[1] Y6, FINIC, Y6:FINIC pristine film and PM6:acceptor blended film were prepared with optimized conditions, then Al (*ca.* 80 nm) was evaporated under vacuum (*ca.* 10^{-5} Pa). For hole-only devices, the PEDOT: PSS (*ca.* 35 nm) was prepared onto the pre-cleaned ITO glass, then PM6:acceptor blend was prepared with optimized conditions, then Au (*ca.* 80 nm) was evaporated under

vacuum. The mobility was extracted by fitting the current density-voltage curves using space charge limited current (SCLC)[2] with the following equation:

$$J = (9/8)\mu\varepsilon_r\varepsilon_0 V^2 \exp(0.89(V/E_0 d)^{0.5})/d^3 \quad (1)$$

where J is current density, μ is hole or electron mobility, ε_r is relative dielectric constant, ε_0 is permittivity of free space, V is the voltage drop across the device, E_0 is characteristic field, d is the thickness of photovoltaic layer. The thickness of photoactive layer was measured using DektakXT (Bruker).

Grazing incidence wide-angle X-ray scattering (GIWAXS) characterization. GIWAXS measurements were performed at beamline 7.3.3[3] at the Advanced Light Source. Samples were prepared on Si substrates using identical blend solutions as those used in devices. The 10 keV X-ray beam was incident at a grazing angle of 0.12 °- 0.14 °, selected to maximize the scattering intensity from the samples. The scattered x-rays were detected using a Dectris Pilatus 2M photon counting detector.

EL measurement. EL measurements were carried out by direct-current meter (PWS2326, Tectronix) to provide bias voltage for the cells. EL spectra were recorded by the fluorescence spectrometer (KYMERA-328I-B2, Andor technology LTD) with cooled silicon array and indium gallium arsenic detector.

EQE_{EL} measurement. EQE_{EL} was recorded by an in-house-built system, which comprises a standard silicon photodiode (S1337-1010BR, Hamamatsu Electronics), Keithley 2400 source meter and Keithley 6482 picoammeter.

sEQE measurement. A quartz halogen lamp (150 W, LSH-75, Newport) and monochromator (CS260-RG-3-MC-A, Newport) were used to supply adjustable

monochromatic light source, which emits an optical signal through the chopper (3502 Optical Chopper, Newport) at a 173 Hz frequency and focuses on the testing devices. The current was amplified by the front-end current amplifier (SR570, Stanford) and the signal was collected and analyzed by a Phase-locked Amplifier (SR830 DSP Lock-In Amplifier, Stanford).

Energy loss measurement. The energy loss of solar cells can be defined as equation (2),[4,5]

$$E_{loss} = qV_{loss} = E_g - qV_{oc} \quad (2)$$

$$= (E_g - qV_{oc,sq}) + (qV_{oc,sq} - qV_{oc,rad}) + qV_{oc,non-rad}$$

$$= \Delta E_1 + \Delta E_2 + \Delta E_3$$

where q is the elementary charge, $V_{oc,\,sq}$ is the maximum voltage by the Shockley–Queisser limit. $V_{oc,\,rad}$ is the open-circuit voltage when there is only radiative recombination, and $V_{oc,\,non\text{-}rad}$ is the voltage loss of non-radiative recombination which is determined by electroluminescence external quantum efficiencies (EQE_{EL}) of the OSCs through the equation (3),

$$\Delta V_{oc,non-rad} = \frac{kT}{q} ln(EQ\,E_{EL}^{-1}) \quad (3)$$

where q is the elementary charge, k is the Boltzmann constant, T is the absolute temperature in Kelvin.

We will now use the principle of detailed balance to make a connection between the low-energy, charge-transfer-dominated part of the sensitive EQE (sEQE) spectra and EL spectra, and to relate these spectra to V_{OC}. Integrating the sEQE spectra over energy and multiplication with q yields the radiative emission current density that follows a diode law

with the radiative saturation current density given by:

$$J_{0,rad} = q \int_{-\infty}^{\infty} sEQE(E)\emptyset_{BB}(E)d(E) \tag{4}$$

$\emptyset_{BB}(E)$ denotes the blackbody spectrum at temperature T of the cell, k is Boltzmann's constant, and q the elementary charge. Then, the radiative limit $V_{oc,rad}$ can then be consistently described using the equation (5):

$$V_{oc,rad} = \frac{nkT}{q} ln\left(\frac{J_{sc}}{J_{0,rad}}\right) \tag{5}$$

Here n is the radiative ideality factor.

The in-situ film-depth-dependent light absorption spectra characterization. The in-situ film-depth-dependent light absorption spectra[6] were measured through PG-2000 (Ideaoptics Instruments) combining with a plasma etching process which was carried out by a home-made soft plasma generator with the pressure below 30 Pa and operating frequency of 13.56 MHz.

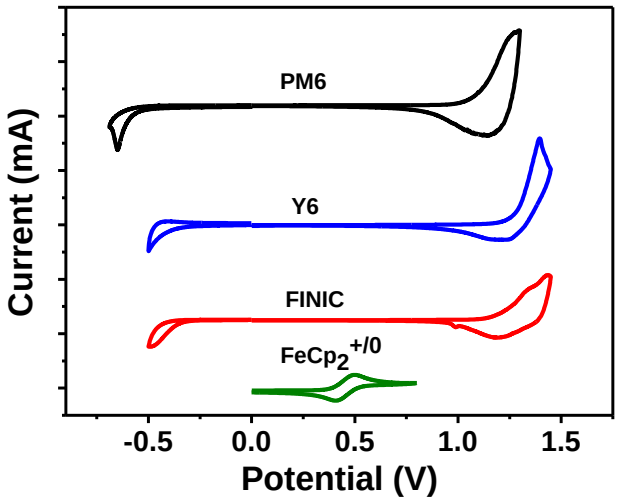

Fig. S1 Cyclic voltammograms of PM6, Y6 and FINIC in CH_3CN / 0.1 M $[^nBu_4N]^+[PF_6]^-$ at 100 mV s^{-1}, and the horizontal scale refers to an Ag/AgCl electrode.

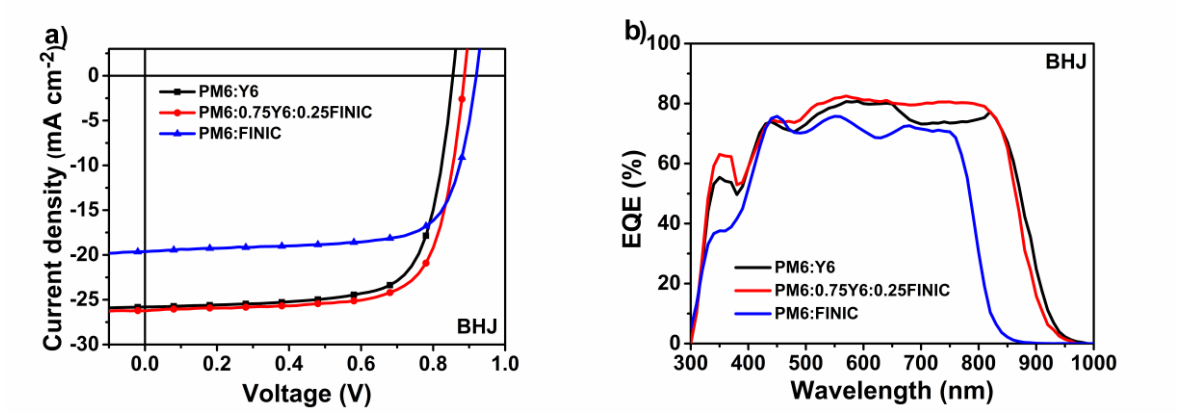

Fig. S2 (a) *J*-*V* characteristics and (b) EQE spectra of the BHJ OSCs based on PM6:acceptor.

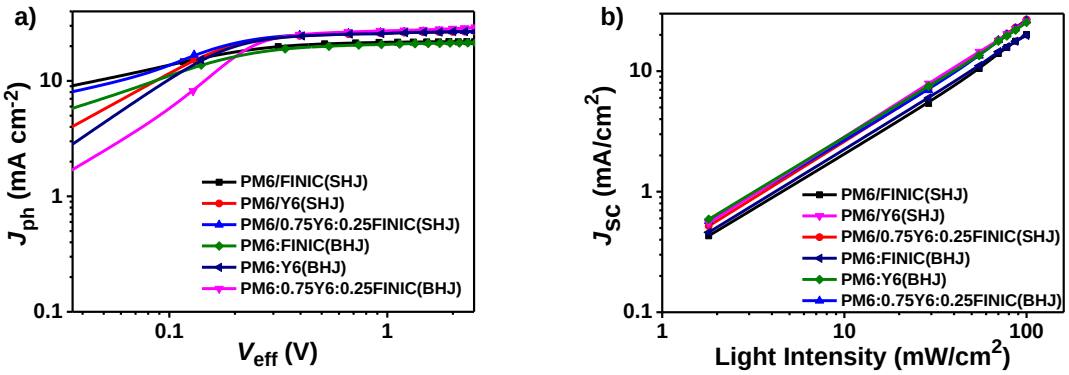

Fig. S3 (a) J_{ph} versus V_{eff} characteristics and (b) J_{sc} versus light intensity of the FINIC-, Y6- and Y6:FINIC-based SHJ and BHJ blends under optimized condition.

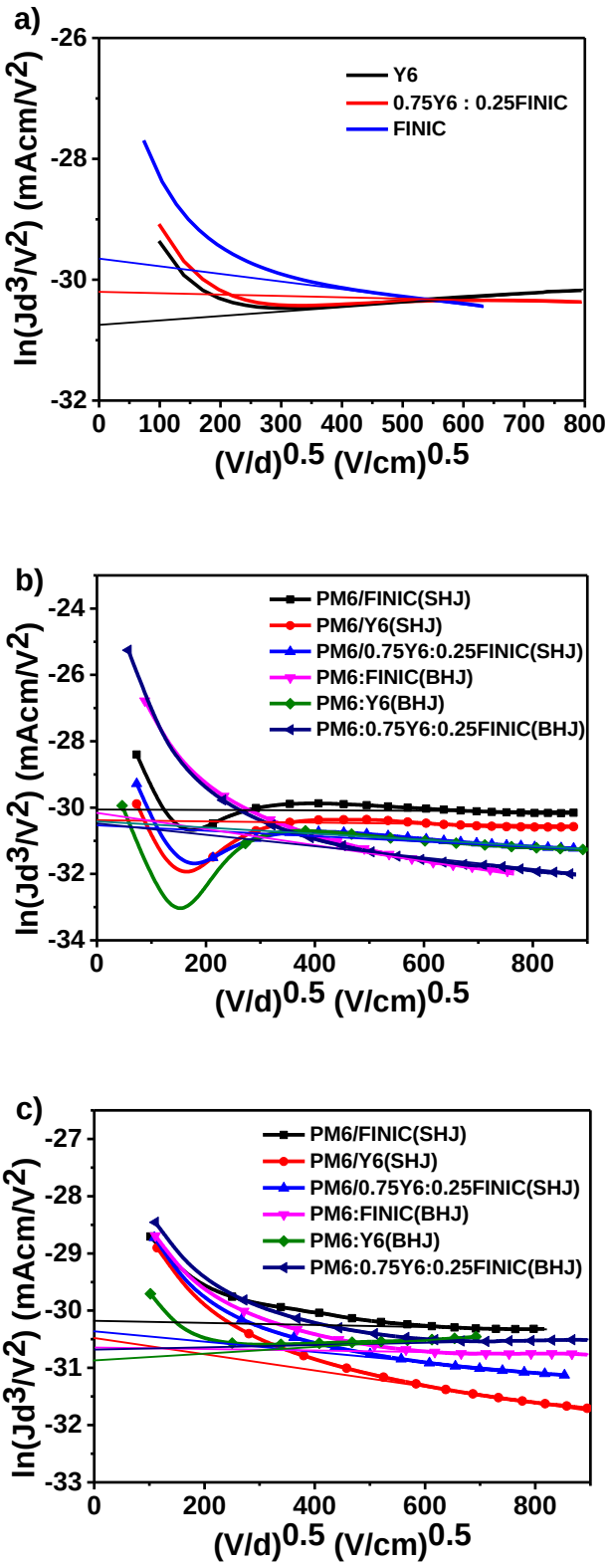

Fig. S4 *J-V* characteristics in the dark for electron-only devices based on Y6, Y6:FINIC and FINIC pristine films (a), for hole-only (b) and electron-only (c) devices based on FINIC-, Y6- and Y6:FINIC- SHJ and BHJ blends under optimized condition.

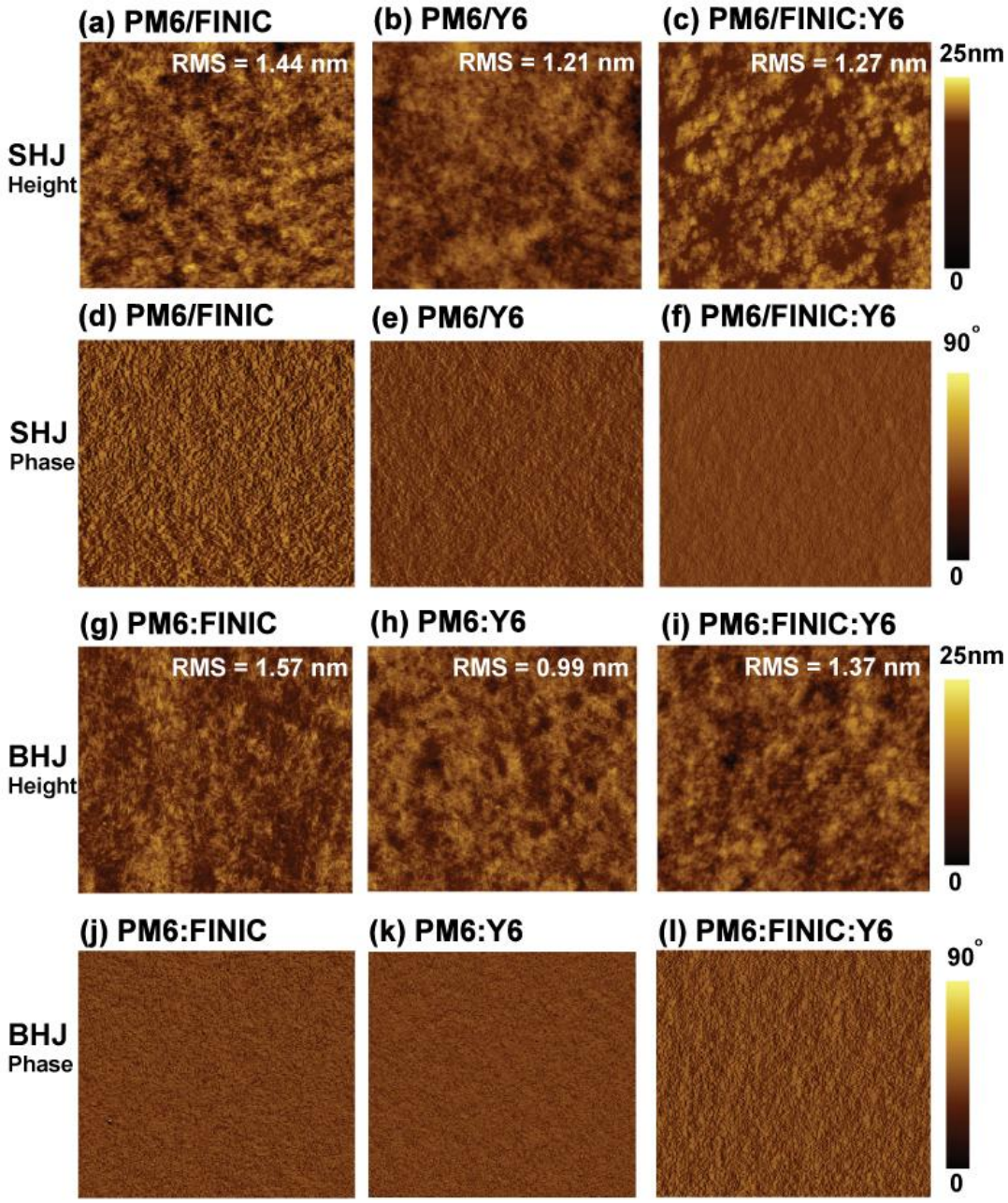

Fig. S5 AFM height (a-c) and phase (d-f) images of SHJ films: PM6/FINIC (a and d), PM6/Y6 (b and e), PM6/FINIC:Y6 (c and f). AFM height (g-i) and phase (j-l) images of BHJ films: PM6:FINIC (g and j), PM6:Y6 (h and k), PM6:FINIC:Y6 (i and l). All films were prepared under optimized condition. The scales of images are 2.0 μm × 2.0 μm.

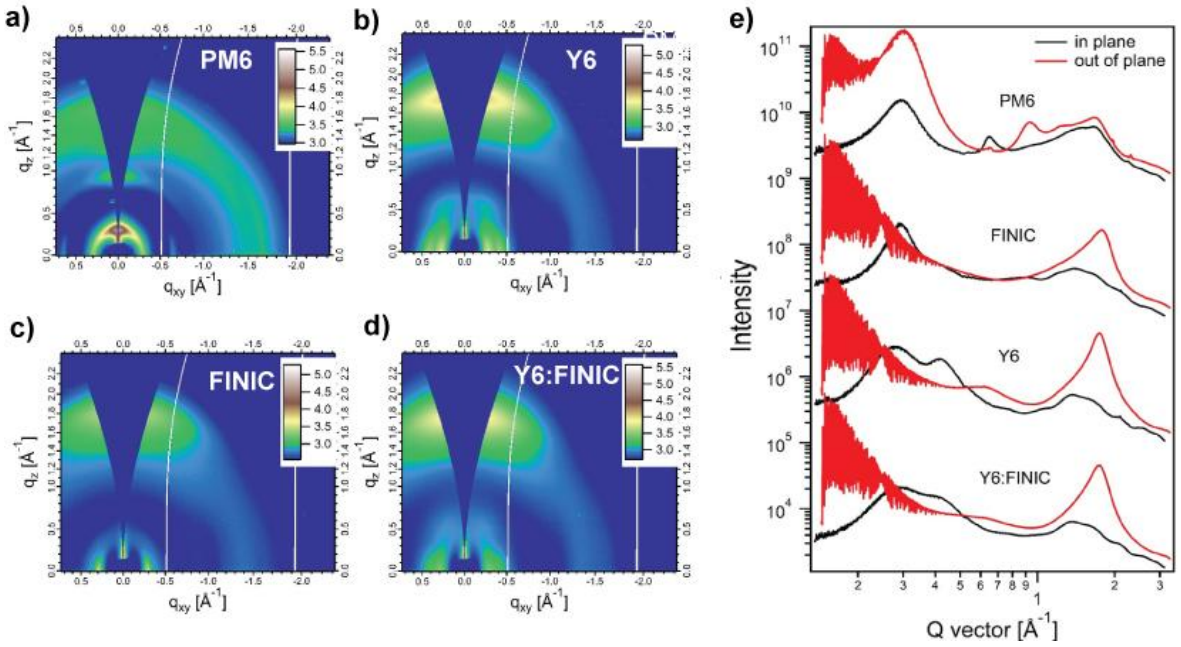

Fig. S6 2D GIWAXS patterns for (a) PM6, (b) Y6, (c) FINIC, (d) Y6:FINIC and (e) 1D line-cuts for pristine donor and acceptor films.

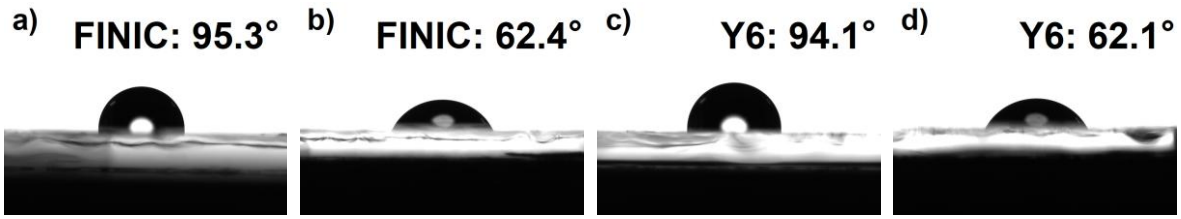

Fig. S7 Contact angle images of FINIC and Y6 films using water (a and c) and ethylene glycol (b and d) as the testing liquids.

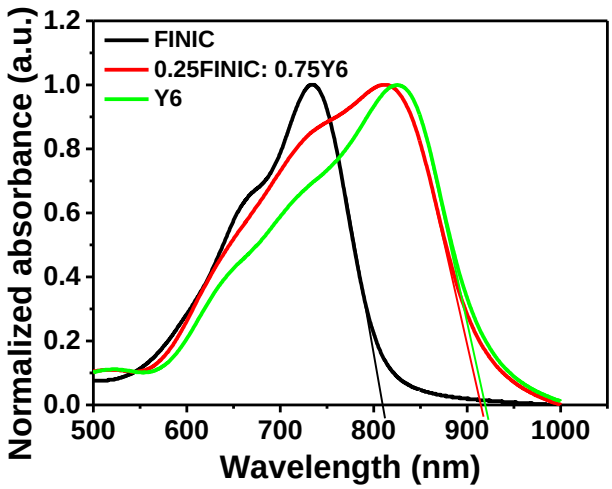

Fig. S8 Absorption edge of Y6 (λ_{edge} = 917.8 nm), FINIC (λ_{edge} = 809.4 nm) and Y6:FINIC (λ_{edge} = 914.5 nm) pristine films.

Table S1 Performance of the SHJ OSCs based on PM6/acceptor with different FINIC ratio (0.15% CN)[a]

acceptor	V_{OC} (V)	J_{SC} (mA cm^{-2})	calc. J_{SC} (mA cm^{-2})	FF (%)	PCE (%)
Y6	0.858	25.8	24.7	73.5	16.3
	(0.857±0.003)	(26.0±0.3)		(72.4±1.5)	(16.1±0.2)
0.75Y6:0.25FINIC	0.887	26.8	25.5	74.7	17.8
	(0.881±0.006)	(26.7±0.5)		(74.0±1.6)	(17.4±0.4)
0.5Y6:0.5FINIC	0.910	23.6	22.7	70.1	15.1
	(0.907±0.003)	(23.8±0.4)		(68.2±2.0)	(14.7±0.4)
0.25Y6:0.75FINIC	0.918	21.4	20.4	73.3	14.4
	(0.919±0.002)	(21.6±0.2)		(72.2±1.5)	(14.3±0.2)
FINIC	0.925	19.5	19.2	74.4	13.4
	(0.927±0.004)	(19.9±0.4)		(72.3±2.0)	(13.3±0.3)

[a] The average and deviation values of 10 devices are in the brackets.

Table S2 Performance of the SHJ OSCs based on PM6/0.75Y6:0.25FINIC with different CN ratio[a]

CN (v/v)	V_{OC} (V)	J_{SC} (mA cm^{-2})	FF (%)	PCE (%)
0	0.890	26.4	70.9	16.7
	(0.892±0.003)	(26.1±0.3)	(70.5±1.9)	(16.4±0.3)
0.15	0.887	26.8	74.7	17.8
	(0.881±0.006)	(26.7±0.2)	(74.0±1.6)	(17.4±0.4)
0.25	0.883	27.0	72.5	17.3
	(0.880±0.003)	(26.8±0.3)	(72.3±1.2)	(17.1±0.2)
0.4	0.870	26.5	70.5	16.3
	(0.865±0.006)	(26.5±0.2)	(69.8±2.0)	(16.0±0.3)

[a] The average and deviation values of 10 devices are in the brackets.

Table S3 Device data of BHJ OSCs based on PM6:Y6:FINIC with different FINIC weight ratio (0.15% CN, v/v) [a]

acceptor	V_{OC} (V)	J_{SC} (mA cm^{-2})	calc J_{SC} (mA cm^{-2})	FF (%)	PCE (%)
Y6	0.855 (0.855±0.004)	25.7 (25.4±0.4)	24.5	72.7 (72.3±0.5)	16.0 (15.7±0.4)
0.75Y6:0.25FINIC	0.886 (0.884±0.009)	26.2 (26.5±0.6)	25.1	72.8 (71.3±1.7)	16.9 (16.7±0.3)
FINIC	0.920 (0.926±0.006)	19.6 (19.3±0.3)	19.0	72.9 (72.3±1.0)	13.1 (12.9±0.2)

[a] The average and deviation values of 10 devices are in the brackets.

Table S4 Hole and electron mobilities of the optimized films

		μ_h (cm^2 V^{-1} s^{-1})	μ_e (cm^2 V^{-1} s^{-1})	μ_h/μ_e
	Y6	-	2.7×10^{-4}	-
	Y6:FINIC	-	4.5×10^{-4}	-
	FINIC	-	8.4×10^{-4}	-
SHJ	PM6/Y6	3.9×10^{-4}	3.2×10^{-4}	1.2
	PM6/0.75Y6:0.25FINIC	3.5×10^{-4}	3.7×10^{-4}	0.95
	PM6/FINIC	4.9×10^{-4}	4.5×10^{-4}	1.1
BHJ	PM6:Y6	3.7×10^{-4}	2.1×10^{-4}	1.8
	PM6:0.75Y6:0.25FINIC	3.4×10^{-4}	2.6×10^{-4}	1.3
	PM6:FINIC	4.6×10^{-4}	2.7×10^{-4}	1.7

Table S5 Summary of the lamellar and π–π stacking peak position, *d*-spacing and CL of π–π stacking of pristine and blended films

		lamellar ($Å^{-1}$)	π–π stacking ($Å^{-1}$)	*d*-spacing (Å)	CL (nm)
pristine	PM6	0.29	1.68	3.74	1.6
	Y6	0.28	1.74	3.61	2.5
	Y6:FINIC	0.28	1.75	3.59	2.5
	FINIC	0.29	1.78	3.53	2.3
SHJ	PM6/Y6	0.30	1.73	3.63	2.7
	PM6/Y6:FINIC	0.29	1.74	3.61	2.7
	PM6/FINIC	0.29	1.73	3.63	2.2
BHJ	PM6:Y6	0.30	1.72	3.65	2.8
	PM6:Y6:FINIC	0.29	1.75	3.60	2.8
	PM6:FINIC	0.29	1.75	3.60	2.3

Table S6 Energy loss analysis on Y6-, Y6:FINIC- and FINIC-based SHJ and BHJ devices

	acceptor	E_g (eV)	qV_{OC} (eV)	E_{loss} [a] (eV)	ΔE_1 [b] (eV)	ΔE_2 [c] (eV)	ΔE_3 [d] (eV)	EQE_{EL}
SHJ	Y6	1.351	0.858	0.493	0.252	0.017	0.224	1.3×10^{-4}
	Y6:FINIC	1.356	0.887	0.469	0.255	0.002	0.212	2.1×10^{-4}
	FINIC	1.532	0.925	0.607	0.266	0.017	0.324	2.3×10^{-6}
BHJ	Y6	1.351	0.855	0.496	0.252	0.006	0.238	7.5×10^{-5}
	Y6:FINIC	1.356	0.886	0.470	0.255	0.009	0.206	2.7×10^{-4}
	FINIC	1.532	0.920	0.612	0.266	0.061	0.285	1.1×10^{-5}

[a] $E_{loss} = q\Delta V$, [b] $\Delta E_1 = E_g - q\Delta V_{OC,sq}$, [c] $\Delta E_2 = q\Delta V_{OC,sq} - q\Delta V_{OC,rad}$, [d] $\Delta E_3 = q\Delta V_{OC,non\text{-}rad}$

References

1 S. Dai, J. Zhou, S. Chandrabose, Y. Shi, G. Han, K. Chen, J. Xin, K. Liu, Z. Chen, Z. Xie, W. Ma, Y. Yi, L. Jiang, J. M. Hodgkiss and X. Zhan, *Adv. Mater.*, 2020, **32**, 2000645.

2 G. G. Malliaras, J. R. Salem, P. J. Brock and C. Scott, *Phys. Rev. B*, 1998, **58**, 13411-13414.

3 A. Hexemer, W. Bras, J. Glossinger, E. Schaible, E. Gann, R. Kirian, A. MacDowell, M. Church, B. Rude and H. Padmore, *J. Phys. Conf. Ser.*, 2010, **247**, 012007.

4 J. Yao, T. Kirchartz, M. S. Vezie, M. A. Faist, W. Gong, Z. He, H. Wu, J. Troughton, T. Watson, D. Bryant and J. Nelson, *Phys. Rev. Appl.*, 2015, **4**, 014020.

5 J. Liu, S. Chen, D. Qian, B. Gautam, G. Yang, J. Zhao, J. Bergqvist, F. Zhang, W. Ma, H. Ade, O. Inganäs, K. Gundogdu, F. Gao and H. Yan, *Nat. Energy*, 2016, **1**, 16089.

6 Z. Wang, Y. Hu, T. Xiao, Y. Zhu, X. Chen, L. Bu, Y. Zhang, Z. Wei, B. B. Xu and G. Lu, *Adv. Opt. Mater.*, 2019, **7**, 1900152.